Prabha Materials Science Letters
Vol. 1, No. 1, 11-20, 2022
https://doi.org/10.33889/PMSL.2022.1.1.003

# Zinc Selenide (ZnSe) for Supercapacitor and Photocatalytic Applications

**S. Pavithra**
Solid State Ionics Lab, Department of Applied Physics,
Karunya Institute of Technology and Sciences, Coimbatore-641 114, Tamil Nadu, India.

**C. Joelin**
Solid State Ionics Lab, Department of Applied Physics,
Karunya Institute of Technology and Sciences, Coimbatore-641 114, Tamil Nadu, India.

**S. Rajesh**
Solid State Ionics Lab, Department of Applied Physics,
Karunya Institute of Technology and Sciences, Coimbatore-641 114, Tamil Nadu, India.
E-mail: drsrajesh@karunya.edu

**A. Sakunthala**
Solid State Ionics Lab, Department of Applied Physics,
Karunya Institute of Technology and Sciences, Coimbatore-641 114, Tamil Nadu, India.
*Corresponding author*: sakunthala@karunya.edu

(Received on April 26, 2022; Accepted on May 25, 2022)

**Abstract**
Commercial Zinc Selenide (ZnSe) was explored as an electrode material for aqueous supercapacitor systems. The material was found to have a cubic structure with no impurities and hence as such subjected to the electrochemical properties in a three electrode system. The material was found to deliver a first cycle discharge capacitance of 106 F/g for a current density of 0.125A/g in the wide potential window of -0.8 to 0.5 V. The cycling efficiency of the commercial material was tested at a high current rate of 3 A/g. The material delivered a discharge capacitance of 16 F/g even after 1000 cycles. The used electrode after 1000 cycles was then explored for the photocatalytic efficiency. The dye degradation was about 78.96 % for methylene blue, indicating ZnSe to be a promising material for both the energy and environmental applications.

**Keywords**- Zinc selenide, Aqueous supercapacitor, Photocatalysis, Dye degradation, Environment.

## 1. Introduction

The universe is in need of clean and renewable energy storage systems for the pollution free environment (Kumar and Majid, 2020). The supercapacitors are considered as the promising energy storage devices as they have high power density like capacitors and high energy density like batteries (Olabi et al., 2022). Though the non-aqueous supercapacitors have higher energy density, the electrolytes used are toxic and not safe in nature. Where else, the aqueous supercapacitors are very promising in nature in terms of safety features (Zhao and Zheng, 2015). The main drawback of the aqueous supercapacitors is the voltage limitations owing to the decomposition of water over 1.23 V. Hence, the materials with higher over potential for hydrogen evolution can be utilised in order to overcome the water splitting. In this sense, many bimetallic selenides were explored as the materials for supercapacitor applications (Wu et al., 2018; Cheng et al., 2020; Moosavifard et al., 2020). Yet to the best of the author's knowledge, the exploration of the ZnSe for the supercapacitor applications and its morphological stability or degradation during long cycling is not reported elsewhere. The Zinc Selenide with two different crystal structures like hexagonal (wurzite) and cubic (zinc blende) has an application as a material for light emitting diodes and for diode

lasers (Chen et al., 2005; Huang et al., 2021). The material being insoluble in water can be explored as a suitable material for aqueous supercapacitor applications, which is the aim of the present report. The material was explored as supercapacitor electrode material in aqueous electrolyte system to get its electrochemical signature. The electrochemical properties suggest that, it has pseudo capacitor behaviour rather than electric double layer capacitor behaviour. The used material after long cycles of charge and discharge process, was found to have excellent photocatalyst property. The structural and morphological properties of the used electrode was found to influence the photocatalytic property.

## 2. Experimental Techniques

Zinc Selenide (ZnSe) was purchased from Sigma Aldrich. The slurry for working electrode was done by grinding ZnSe, activated carbon and PVDF in ratio80:10:10. NMP was used as solvent (Figure 1). Graphite sheet was used as current collector. The coated electrodes were dried for 24 hrsat 80°C.Three electrode set up with slurry coated graphite sheet as the working electrode, Ag/AgCl as reference and platinum wire as a counter electrode in 1M KOH aqueous electrolyte was arranged (Pavithra et al., 2021).

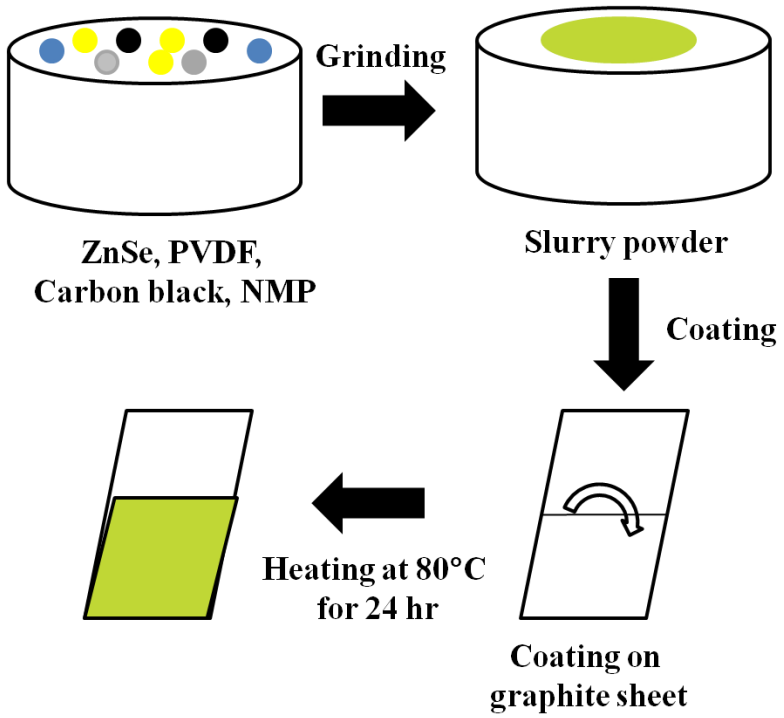


**Figure 1.** Schematic representation of electrode preparation.

X-ray Diffraction patterns of the sample were obtained using a SHIMADZU-XRD-6000 diffractometer with Cu-Kα radiation (wavelength = 0.1541 nm) as the source at 40 kV with a scanning range between 5° and 80° at 10°/min scan speed. Scanning Electron Microscope (SEM) wasdone using JEOL-JSM 6000 for morphology analysis. UV-Vis-NIR Spectrophotometer, V-670 in the wavelength range of 400-800 nm was used for optical studies. Computer controlled CH electrochemical workstation (Model: CHI-6008E) were used to record electrochemical studies. Cyclic Voltammetry (CV) was measured in the potential range of -0.8 to 0.6 V at various scan rates; The Galvanostatic Charge Discharge (GCD) in the range of -

0.8 to 0.5V were done at current densities of 0.125, 0.25, 0.5, and 1 to 10A/g. Specific capacitance obtained from CV was calculated using the formula (Pavithra et al., 2021).

$$C = \frac{A}{2kmΔV} \quad (1)$$

where, 'C' - specific capacitance, 'A' - area under the CV curve, 'k' - scan rate, 'm' - mass of electrode and ΔV - potential difference. Specific capacitance obtained from GCD was calculated using the formula (Pavithra et al., 2021).

$$C = \frac{I * \Delta t}{m * \Delta V} \quad (2)$$

where 'C' - specific capacitance in F/g, 'I' - current density, 'Δt' - time of discharge, m' - mass of electrode and ΔV - potential difference. The photocatalytic measurement was made using Philips 250 W low voltage halogen lamp as the optical source. The methylene blue dye (MB) ($C_{16}H_{18}ClN_3S$) was used for the photocatalyst dye degradation studies.

## 3. Results and Discussion

### 3.1 XRD Analysis

Figure 2 shows the XRD pattern for the commercial Zinc Selenide. The characteristics peaks of ZnSe were found at 2θ = 27.1°, 45.1°, 53.4°, 65.7° and 72.5° which corresponds to (1 1 1), (2 2 0), (3 1 1), (4 0 0) and (3 3 1) hkl planes, respectively. The XRD pattern matches well with the JCPDS card number 88-1360. The commercial ZnSe showed cubic structure (face centered) with the space group of $F\bar{4}3m$.The average crystalline size was calculated to be 205 nm.

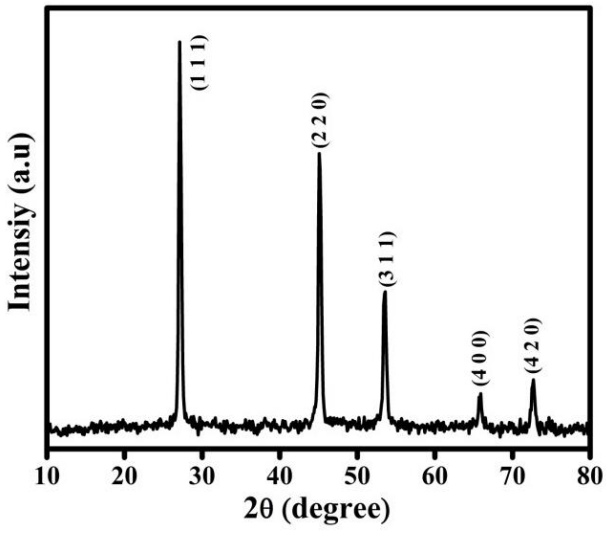


**Figure 2.** XRD pattern for commercial ZnSe powder.

Solubility nature of commercial zinc, selenium and Zinc Selenide powder materials (left to right) were tested as shown in Figure 3. It can be seen that Zinc, Selenium and Zinc Selenide particles shows very poor solubility in the water.

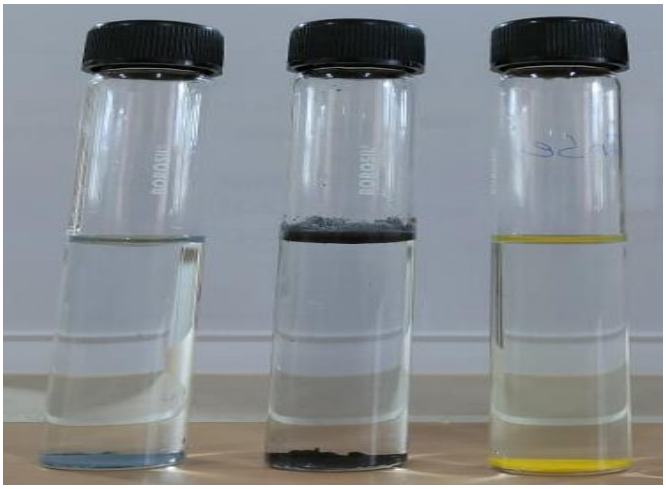

**Figure 3.** Solubility behaviors of (left to right) pure zinc, pure selenium and ZnSe.

## 3.2 Electrochemical Studies

### 3.2.1 Cyclic Voltammetery Studies

Cyclic Voltammetry (CV) was measured in -0.8 to 0.6V potential range using three electrode systems as shown in Figure 4(a). The specific capacitance of the ZnSe electrode was found to be 15.77, 17.33, 19.53, 22.89, 29.52, 37.21 and 46.65 F/g at the scan rate of 100, 80, 60, 40, 20, 10 and 5 mV $s^{-1}$ (Figure 4b). The increase in specific capacitance value with decrease in scan rate is due to the sufficient time given for the ions to interact (Sarkar and Khan, 2018). Also the current value increases with increase in the scan rate as the growth of diffusion layer is constricted at higher scan rates which leads to the higher electrolyte flux (Sarkar et al., 2015). It has been noted that no dissolution of ZnSe from the electrode into the electrolyte solution even after the long use of the electrode. This is due to the insolubility nature of ZnSe in water and therefore ZnSe is suitable for energy storage devices with aqueous electrolytes.

The charge discharge storage kinetics were measured using the CV graph using the relationship between current ($i$) and scan rate ($\vartheta$) as follows (Teli et al., 2020)

$$i = a\vartheta^b \tag{3}$$

where, '$I$' is the current at specific voltages; '$\vartheta$' is the scan rate; 'a' and 'b' are constants. Figure 4c shows the dependence of peak current on the scan rate and corresponding 'b' values. The 'b' value between 0.5 and 1 in the cathodic and anodic peak represents both diffusion and capacitive controlled behaviour of the material (Teli et al., 2020).The cathodic and anodic peaks show the 'b' values of 0.7 and 0.5, respectively. Therefore, the total current of the ZnSe is contributed by both the diffusion controlled charge storage and surface controlled capacitive behaviour.

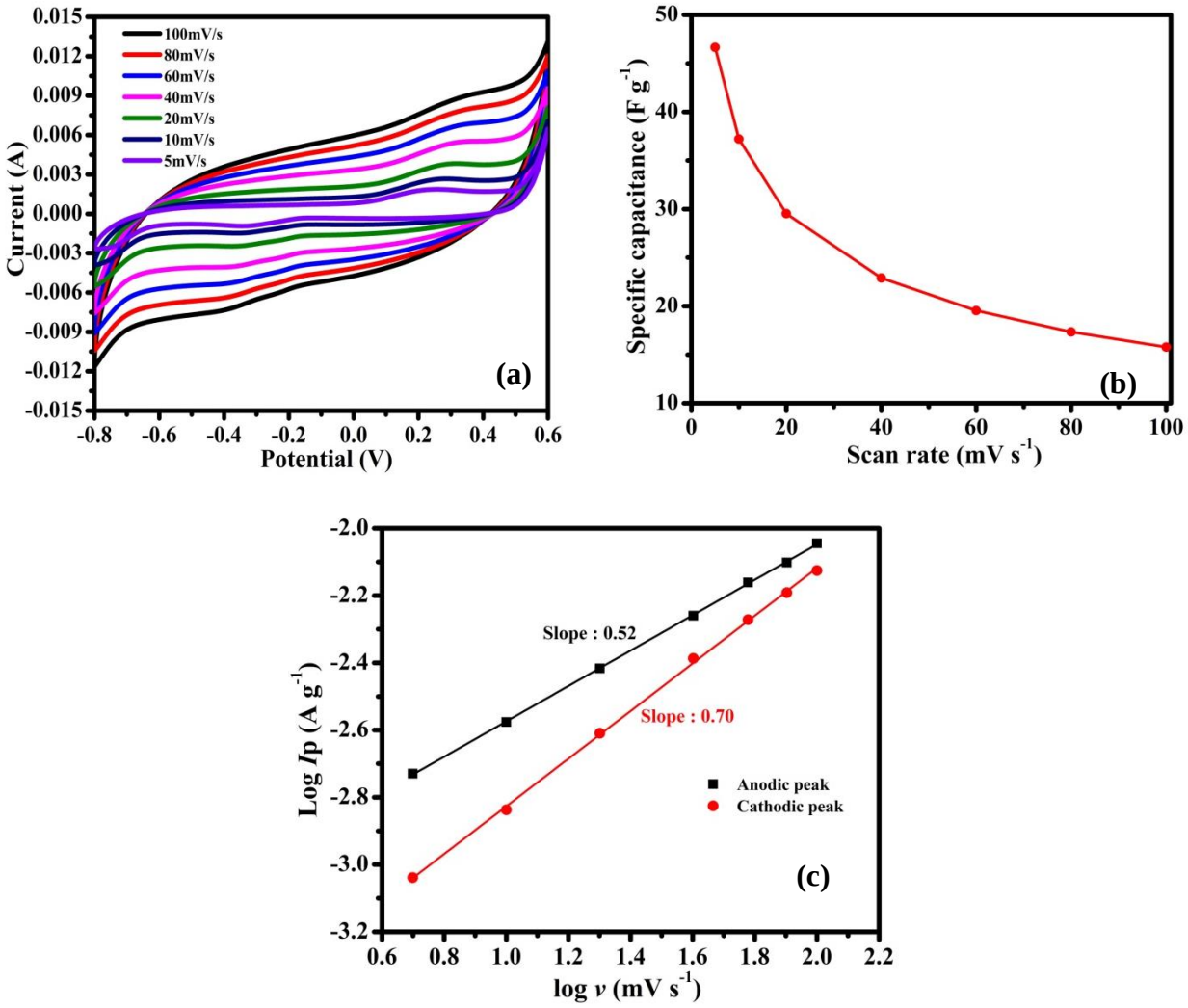


**Figure4.** (a) CV curves of ZnSe electrode at different scan rates (b) Scan rate (vs.) specific capacitance (c) dependence of peak current on the scan rate.

### 3.2.2 Galvanostatic Charge- Discharge Studies

Galvanostatic charge discharge studies were carried out in the potential range of -0.8 to 0.5V at different current densities. Comparison of ZnSe electrode at different current densities was shown in Figure 5a.

The GCD curve of the ZnSe electrode shows the pseudocapacitor behaviour. As the current density increases specific capacitance was found to decrease. The specific capacitance of the ZnSe electrode was found to be 106.87, 88.04, 75.04, 63.76, 21.53, 19.15, 12.61, 10.76, 8.07 and 4.61 F $g^{-1}$at the current densities of 0.125, 0.25, 0.5, 1, 2, 3, 4, 5, 7, 10 A $g^{-1}$, respectively. Cyclic stability was tested for ZnSe electrode for 1000 cycles at the current density of 3A $g^{-1}$ (Figure 5c). The 1$^{st}$ and 1000$^{th}$cycle showed a specific capacitance of 19 and 16 F $g^{-1}$, respectively. It was seen that ZnSe shows 85% retention of specific capacitance after 1000 cycles at high current density of 3A$g^{-1}$. The increase in capacitance was observed from 200$^{th}$ cycle.

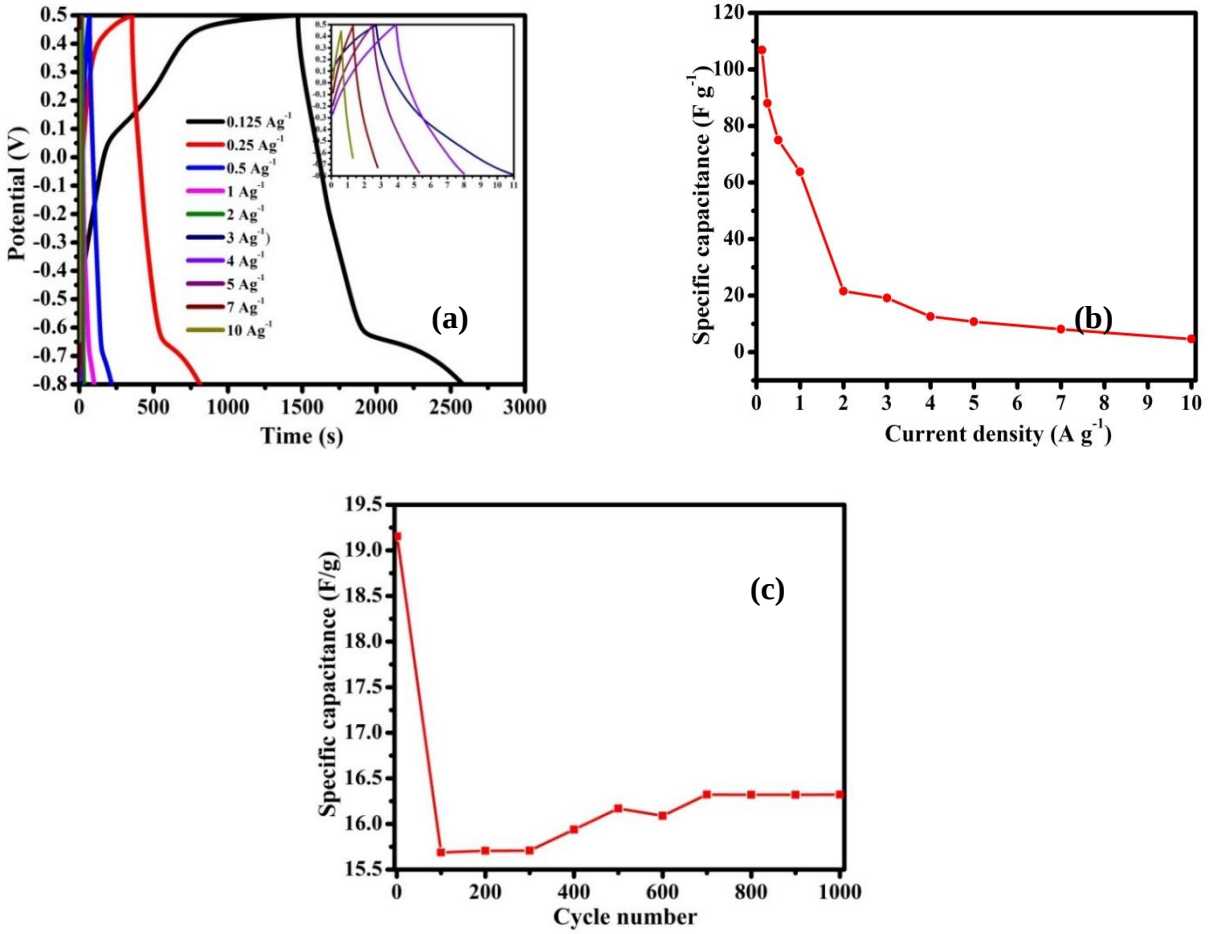


**Figure5.** (a) GCD curves (first cycle) of ZnSe electrode at different current density (b) Different current density (vs.) specific capacitance (c) Cyclic stability for 1000 cycles at current density of 3A $g^{-1}$.

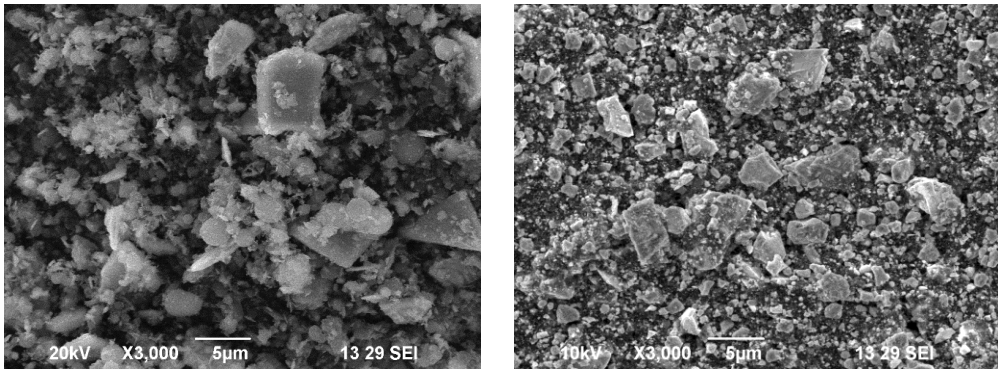


(a) (b)

**Figure 6.** SEM images of ZnSe electrode taken (a) before cycling and(b) after 1000 charge-discharge cycles (current density of 3 A $g^{-1}$).

Figure 6 shows the SEM images of the ZnSe electrode before and after 1000 cycles at current density of 3 A $g^{-1}$. It was found that the ZnSe particles in the electrodes has undergone electrochemical grinding and a size reduction due to long cycles. This has enhanced the charge/discharge capacitance of the material beyond 200 cycles. Hence this material is found to be promising with a size reduction by preparation through chemical routes.

### 3.2.3 Electrochemical Impedance Spectroscopy (EIS) Analysis

EIS analysis was done to observe the capacitive and resistive behaviors in the frequency range of 1 mHz to 1kHz for ZnSe electrode. The absence of semicircle at high frequency region and presence of spike in the low frequency region is evident that the material shows capacitive nature with low internal resistance (Poudel et al. 2020). There was no much increase in the resistance after 1000 cycles, owing to the electrochemical grinding of the ZnSe particles.

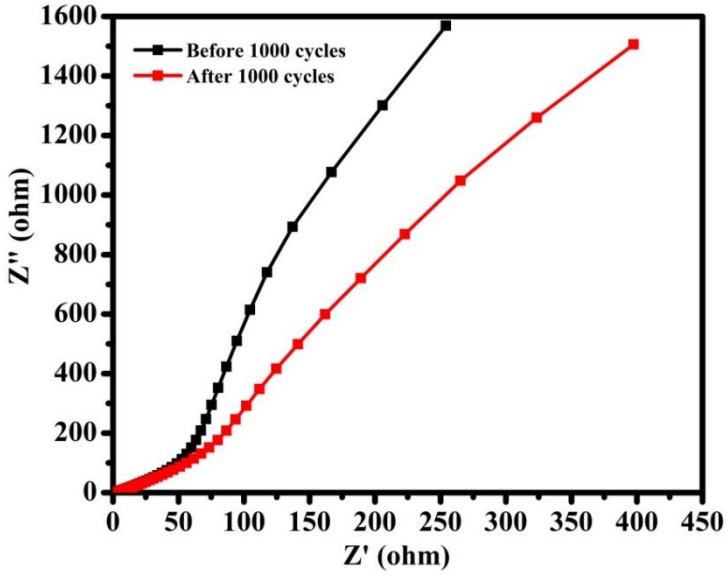


**Figure7.** EIS studies of ZnSe electrode (a) before cycling and (b) after 1000 cycles of charge-discharge at current density of 3 A $g^{-1}$.

### 3.3 Photocatalytic Studies

The ZnSe working electrode after its use in the three electrode system was taken as such and dried in ambient atmosphere for some time. Later the dried electrode of mass 3 mg was tested for photocatalytic degradation under visible light. Methylene blue dye was used to test the photocatalytic degradation effect on the used electrode in the concentration of 20 mg $L^{-1}$ with the pH maintained at 6.5. The commercial ZnSe powder of 3 mg was tested for comparison. The aqueous solution with methylene blue and the photocatalyst was taken in a 100 ml beaker and stirred continuously. First the solution was stirred in dark for 30 min followed by stirring in the presence of visible light. The samples were collected at regular intervals of every 30min to test the degradation property using UV-Vis spectrometer. The absorbance spectra were recorded at different time intervals in the range of 400 to800 nm and the absorbance of methylene blue was found at 663 nm. Figure 8 (a-b) shows the UV-vis absorption spectra of MB solution degraded with commercial ZnSe powder and the used ZnSe electrode. The Figure 8 (c-d) shows their corresponding decolouration pictures, respectively.

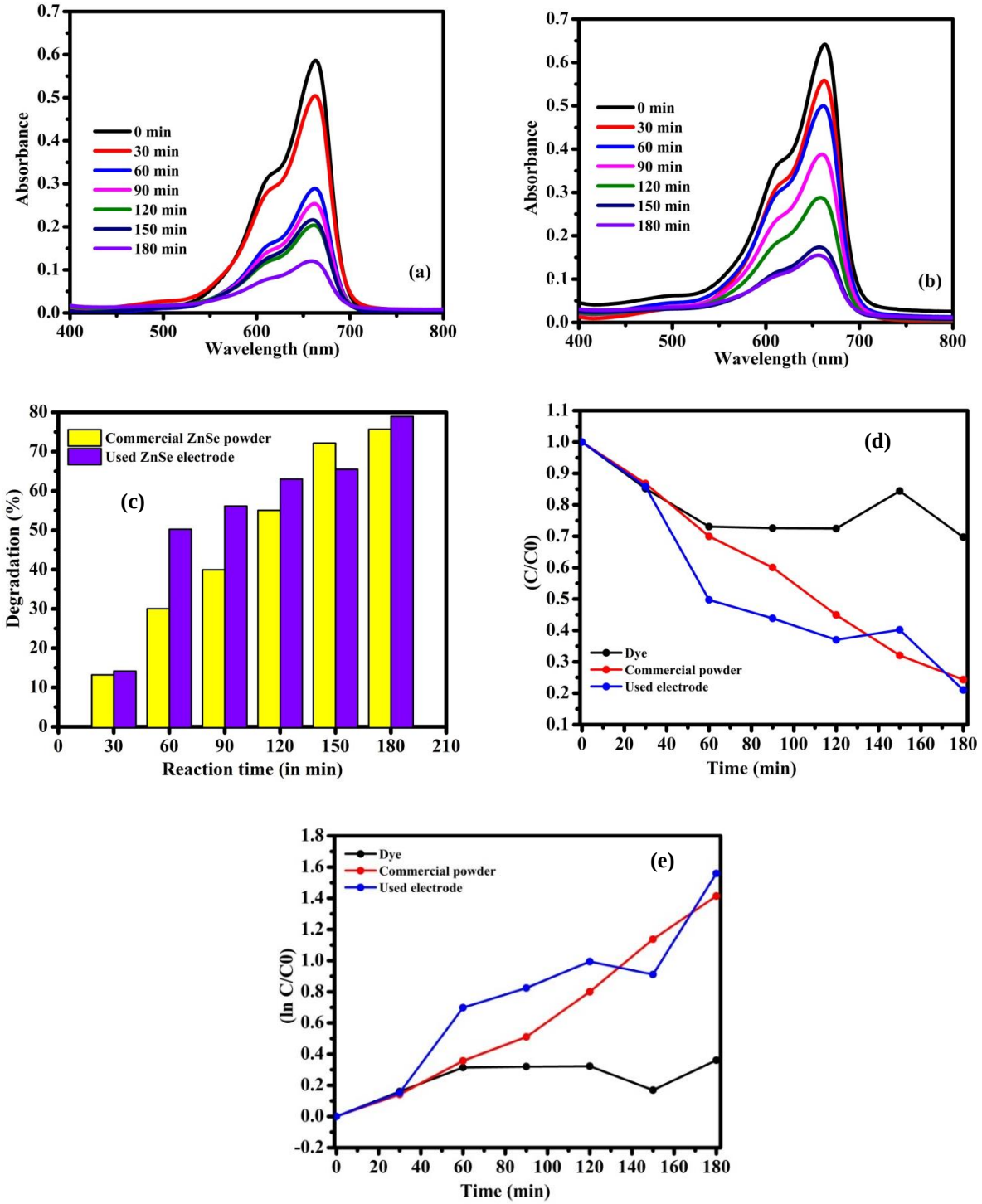


**Figure 8.** UV absorbance spectra of MB solution in case of (a) used ZnSe electrode (b) commercial ZnSe powder, (c) Comparison of degradation (%) vs. reaction time (in min)(d) photo degradation efficiency ($C/C_0$) of MB over dye, used ZnSe electrode and commercial ZnSe powder(e) Pseudo-first-order kinetic model fit for the degradation of MB with dye, used ZnSe electrode and commercial ZnSe powder.

The reduction in methylene blue peak at 663 nm confirms the degradation of MB dye using photocatalysts (Figure 8 (a-b)). The percentage of dye degradation was calculated using the formula,

$$\text{Degradation \%} = \left(\frac{A_0 - A}{A_0}\right) \text{x100.} \quad (4)$$

where, 'A' is the initial dye concentration and '$A_0$' is the dye concentration at certain irradiation time. After 0, 30, 60, 90, 120, 150 and 180 minutes, the dye degradation percentage was found to be 0, 14.16, 50.20, 56.15, 63.00, 65.49 and 78.96 % for used ZnSe electrode, whereas it was about 0,13.21, 30.02, 39.95, 55.07, 72.17 and 75.69 % for commercial ZnSe powder. The Figure 8e shows the comparison of degradation % between the two photocatalyst and it can be seen that the electrode used for electrochemical activities shows higher degradation percentage. Langmuir–Hinshelwood model was used to fit the experimental data to find the reaction kinetics of the photocatalytic MB degradation (Guo et al., 2016) as follows

$$\text{Ln (C/C0)} = \text{kt.} \quad (5)$$

where, C and C0 are the concentrations of MB solution at time t and initial concentration, k is the first-order rate constant, respectively. Pseudo first-order kinetics with respect to dye concentration (as shown in Figure 8e was proved by the linear fit between ln(C/Co) and reaction time and the correlation coefficient for dye, commercial powder and used electrode to be $R^2$ = 0.31705, 0.97563 and 0.8835 and k =0.7333x $10^{-6}$ $min^{-1}$, 0.441x $10^{-4}$ $min^{-1}$ and 0.429 x $10^{-4}$ $min^{-1}$ respectively.

## 4. Conclusion

Commercial cubic ZnSe powder was tested for pseudocapacitor application using aqueous three electrode setup. The ZnSe electrode exhibited a high specific capacitance of 106 F/g at 0.125 A/g in the potential window of -0.8 to 0.5 V. Cyclic stability was tested at high current density of 3 A/g and the 85% of specific capacitance retention was achieved after 1000 cycles. The used ZnSe electrode from the three electrode cell was further used as a photocatalyst for methylene blue dye degradation studies. The 78.96 % of dye degradation achieved for the used ZnSe electrode proves it to be a potential material for both the electrochemical and photocatalytic applications.

### Conflict of Interest

No conflicts of interests to this work.

### Acknowledgment

The authors thank the Karunya Institute of Technology and Sciences, Coimbatore 641 114, Tamil Nadu, for the research facilities.

## References

Kumar, C.R.J., & Majid, M.A. (2020). Renewable energy for sustainable development in India: Current status, future prospects, challenges, employment, and investment opportunities. *Energy, Sustainability and Society*, *10*, 1-36. https://doi.org/10.1186/s13705-019-0232-1.

Chen, H.S., Wang, S.J.J., Lo, C.J., & Chi, J.Y. (2005). White-light emission from organics-capped ZnSe quantum dots and application in white-light-emitting diodes. *Applied Physics Letters*, *86*(13), 131905. https://doi.org/10.1063/1.1886894.

Cheng, L., Chen, S., Zhang, Q., Li, Y., Chen, J., & Lou, Y. (2020). Hierarchical sea-urchin-like bimetallic zinc–cobalt selenide for enhanced battery-supercapacitor hybrid device. *Journal of Energy Storage*, *31*, 101663. https://doi.org/10.1016/j.est.2020.101663.

Guo, Y., Li, J., Gao, Z., Zhu, X., Liu, Y., Wei, Z., Zhao, W., & Sun, C. (2016). A simple and effective method for fabricating novel p–n heterojunction photocatalyst g-C3N4/Bi4Ti3O12 and its photocatalytic performances. *Applied Catalysis B: Environmental*, *192*, 57-71. https://doi.org/https://doi.org/10.1016/j.apcatb.2016.03.054.

Huang, F., Ning, J., Duan, Z., Sergeev, A.A., Portniagin, A., Kershaw, S.V., Tian, J., & Rogach, A.L. (2021). Induction of wurtzite to zinc-blende phase transformation in ZnSe nanorods during Cu (I) cation exchange. *Chemistry of Materials*, *33*(7), 2398-2407. https://doi.org/10.1021/acs.chemmater.0c04588.

Moosavifard, S.E., Saleki, F., Mohammadi, A., Hafizi, A., & Rahimpour, M.R. (2020). Construction of hierarchical nanoporous bimetallic copper-cobalt selenide hollow spheres for hybrid supercapacitor. *Journal of Electroanalytical Chemistry*, *871*, 114295. https://doi.org/10.1016/j.jelechem.2020.114295.

Olabi, A.G., Abbas, Q., Al Makky, A., & Abdelkareem, M.A. (2022). Supercapacitors as next generation energy storage devices: Properties and applications. *Energy*, *248*, 123617. https://doi.org/https://doi.org/10.1016/j.energy.2022.123617.

Pavithra, S., Keerthana, S.P., Yuvakumar, R., Kumar, P.S., Rajesh, S., Vidhya, B., & Sakunthala, A. (2021). Preparation of β-FeOOH by ultrasound assisted precipitation route for aqueous supercapacitor applications. *Inorganic and Nano-Metal Chemistry*, 1-7. https://doi.org/10.1080/24701556.2021.1988978.

Poudel, M.B., Yu, C., & Kim, H.J. (2020). Synthesis of conducting bifunctional polyaniline@ Mn-TiO2 nanocomposites for supercapacitor electrode and visible light driven photocatalysis. *Catalysts*, *10*(5), 546. https://doi.org/10.3390/catal10050546.

Sarkar, A., & Khan, G.G. (2018). Synthesis of BiFeO3 nanoparticle anchored TiO2-BiFeO3 nano-heterostructure and exploring its different electrochemical aspects as electrode. *Materials Today: Proceedings*, *5*(3), 10177-10184. https://doi.org/10.1016/j.matpr.2017.11.016.

Sarkar, A., Singh, A.K., Sarkar, D., Khan, G.G., & Mandal, K. (2015). Three-dimensional nanoarchitecture of BiFeO3 anchored TiO2 nanotube arrays for electrochemical energy storage and solar energy conversion. *ACS Sustainable Chemistry & Engineering*, *3*(9), 2254-2263. https://doi.org/10.1021/acssuschemeng.5b00519.

Teli, A.M., Beknalkar, S.A., Pawar, S.A., Dubal, D.P., Dongale, T.D., Patil, D.S., Patil, P.S., & Shin, J.C. (2020). Effect of concentration on the charge storage kinetics of nanostructured MnO2 thin-film supercapacitors synthesized by the hydrothermal method. *Energies*, *13*(22), 6124. https://doi.org/10.3390/en13226124.

Wu, L., Shen, L., Wang, T., Xu, X., Sun, Y., Wang, Y., Zhao, Y., Du, Y., & Zhong, W. (2018). Component-controllable bimetallic nickel cobalt selenides (NixCo1-x) 0.85 Se for high performance supercapacitors. *Journal of Alloys and Compounds*, *766*, 527-535. https://doi.org/10.1016/j.jallcom.2018.06.353.

Zhao, C., & Zheng, W. (2015). A review for aqueous electrochemical supercapacitors. *Frontiers in Energy Research*, *3*, 23. https://doi.org/10.3389/fenrg.2015.00023.